High-resolution acoustic imaging from a borehole to detect a nearby well

Michael Jervis[1], Thierry Tonellot[1], Andrey Bakulin[1], and Ibrahim A. Ghamdi[2]

https://doi.org/10.1190/tle37110812.1.

Abstract

A new imaging application is presented using sonic waveform data for ranging to locate a nearby borehole. The challenge of locating a nearby well from a borehole is commonly addressed with electromagnetic (EM) or passive magnetic ranging methods, which can suffer from poor resolution and penetration and require the presence of a conductive or magnetic casing. In addition, the deeper reading active EM methods do not work well when the two boreholes are orthogonal. In contrast, acoustic imaging requires only an impedance contrast between the target object and the surrounding formation, which is adequately provided by the presence of a fluid-filled borehole, even without casing. Here we use acoustic full-waveform sonic data to identify the location, distance, and direction to a target vertical borehole from a nearby highly deviated observation well. The target borehole was located at a distance of about 9 ft with an accuracy of less than 0.5 ft, which was subsequently confirmed by drilling. In addition, acoustic waveform data made it possible to image up to 100 ft above and below the observation well at a resolution comparable to gamma ray and electric logs from the target well.

Introduction

When trying to locate one borehole from another, the most commonly used methods require the presence of casing that is either magnetic or conductive. Electromagnetic (EM) and magnetostatic tools are both available for ranging. Active EM methods have a good detection range (< 60 m) when the boreholes are relatively parallel, while the ranges of magnetic methods, which rely on remnant magnetism (< 15 m) and magnetized casing joints (25–40 m), are relatively shorter. Many of the active EM methods also rely on access to the target borehole with a sensor or emitter. Acoustic methods were first proposed as a ranging technique by Jervis et al. (2012). These methods only rely on an impedance contrast between the formation and the target borehole, whether cased or uncased, and require access only to the observation borehole.

Imaging using sonic-log data (Figure 1a) is a well-known technique for locating fractures and mapping bed boundaries at distances up to 60 ft away from the well (Hornby, 1989; Esmersoy et al., 1998). In this study, sonic waveform data are used to locate a nearby vertical borehole from a highly deviated observation well. This is an example of single-well seismic imaging, which is defined as acquisition using a seismic source and receivers within the same borehole (Figure 1). Single-well imaging has been used for high-resolution reservoir characterization, well planning, and fault/fracture mapping (Hornby, 1989; Esmersoy et al., 1998; Haldorsen et al., 2006).

Single-well acoustic data are generally acquired using conventional sonic-logging tools. This type of data presents two major challenges for imaging: (1) removal of high-amplitude borehole-related arrivals such as refractions and Stoneley waves and (2) azimuthal wavefield separation so that the direction of the arrivals can be determined. Borehole arrivals are much stronger than the reflection events. Refractions and Stoneley waves are difficult to completely remove due to two factors. First, they commonly swamp reflection arrivals due to their large relative amplitudes (up to 100 times the amplitude of reflections). Second, the small spatial aperture of sonic logs (limited number of traces and limited offset range) reduces the efficiency of any multichannel filtering. Even after the borehole arrivals are removed or attenuated, the reflections need to be separated to discriminate energy coming from different directions above and below the borehole as well as arrivals from 3D heterogeneities to the side of the borehole. In the case of imaging, if there is a sufficient difference between the angle of the reflectors and the logging tool path, *f-k* filtering can be used for wavefield separation. For discontinuities away from the borehole in other directions, different methods must be used to determine the azimuth of the arrivals. Multicomponent receivers could be used to determine the direction of polarization of arrivals, but these are not available in typical borehole sonic tools. Wavefield separation can be performed by using data recorded using azimuthal receivers at each offset. Such data can provide a degree of discrimination between waves arriving from different directions without using parametric wavefield separation (Haldorsen et al., 2006).

In this study, the sonic tool consisted of 13 receiver levels, each equipped with eight azimuthal piezoelectric sensors spaced every 45° around the tool's circumference. This configuration allows signals arriving from different azimuths/directions to be distinguished using their relative amplitudes, and their approximate direction of travel can be determined (Haldorsen et al., 2006). This is critical information at sonic-logging frequencies because the wavelength of the arrivals is so much larger than the radial receiver spacing that time delays from arrivals on different sides of the tool are difficult to determine and thus are not easy to use for determining the arrival azimuth.

Current industry practice in locating nearby wells

A variety of methods can be used to detect the direction and distance to a target borehole from another borehole. These commonly rely on nonseismic techniques such as passive magnetic detection and active EM ranging. These methods all require that the target borehole be cased with some conductive or magnetic material.

[1]Saudi Aramco, EXPEC Advanced Research Center, Dhahran, Saudi Arabia. E-mail: michael.jervis@aramco.com; thierry.tonellot@aramco.com; a_bakulin@yahoo.com.
[2]Saudi Aramco, Workover Department, Dhahran, Saudi Arabia. E-mail: ibrahim.ghamdi.6@aramco.com.

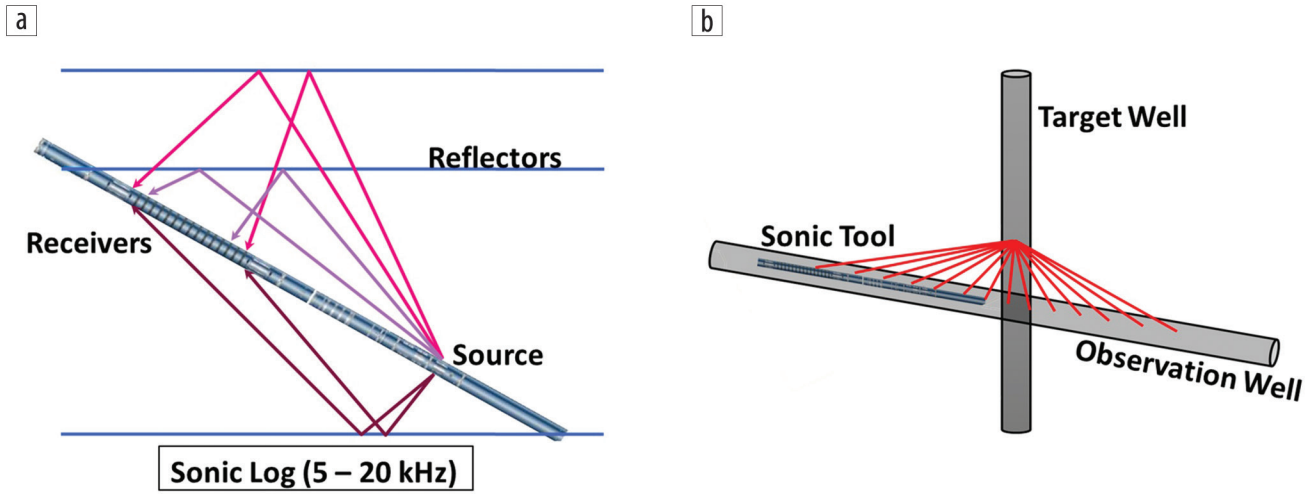

Figure 1. The single-well imaging concept using a sonic logging tool showing (a) sources and receivers in the same borehole and (b) an actual acquisition configuration shown in this study. Note that the receiver array has limited extent due to tool length restrictions.

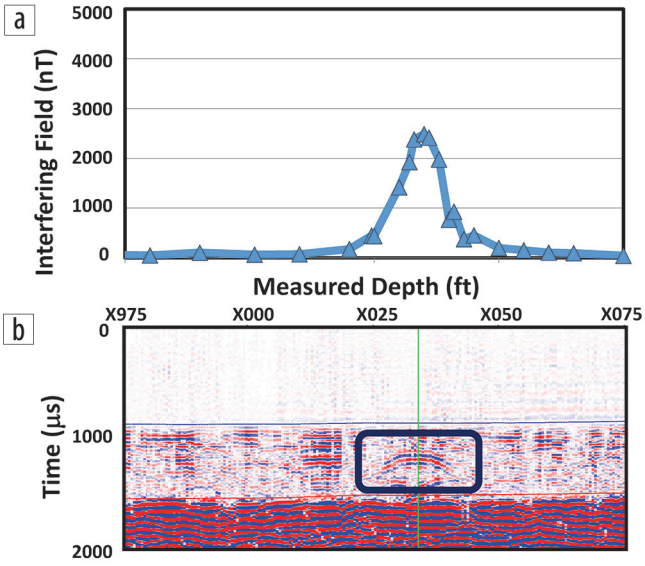

Figure 2. Logging data from the observation well including (a) initial magnetic MWD measurements and (b) a common-offset section of waveform sonic data (17 ft offset) showing a diffraction at the estimated location of the nearby well (dark blue box).

As mentioned earlier, the detection ranges for EM methods are large (typically up to 60 m) and somewhat less for passive magnetostatic tools. The detection range for magnetic methods can be increased by further magnetizing the target casing if access to the target borehole is possible. Since there may be significant uncertainty in the position of both the target and observation wells, these methods are typically the first choice in ranging logging. The formation can also play a role. If magnetic anomalies in the formation are likely to be encountered, magnetostatic methods may be ineffective due to the formation signal masking the casing signal. EM methods also have their limitations. For example, when the formation is anisotropic and dipping with respect to the observation well or when the approach angle between the observation and target well is large, this has two effects. First, EM coupling between the emitter and the target casing is reduced. Second, when the formation resistivity parameters fluctuate significantly over the logging range, EM data can be very difficult to interpret, and signal from the target well may be masked. The advantage is that some EM methods can be run while drilling, which reduces nondrilling or unproductive time. Many EM and magnetic methods still require access to the target borehole to place a magnetic or EM transmitter or receiver, and this is sometimes not possible.

In contrast to EM and magnetic ranging, acoustic methods require only an impedance contrast between the borehole and the formation and do not necessarily require casing. They also do not require access to the target borehole to place a source or receiver. In general, an adequate impedance contrast can be provided by the presence of fluid in the borehole with or without casing. However, acoustic methods are limited by distance due to the source strength and by borehole noise and borehole arrivals present in the data that may mask the reflected signal. Also, like EM methods, where the borehole is at a high angle to bedding, the acoustic signal from the target well may be masked by variations in formation properties.

Field cases

The first example includes magnetic and acoustic measurements from a highly deviated observation well to detect a vertical target well. An observation well was drilled at 75° from the vertical, which passed close to a vertical steel-cased fluid-filled borehole. Measurement-while-drilling (MWD), passive magnetic measurements, sonic full-waveform logging, and later, active EM ranging were used to locate the target well.

Prior to acquisition of the sonic-logging waveform data, passive magnetic measurements were made while drilling to detect the target borehole using remanent magnetization of the casing. Magnetic data suggested that the target was at an azimuth of 270° from the observation well looking along the drilling direction. Magnetic modeling suggested the anomaly or target casing was at a distance of 5.5 ft (Figure 2) from the observation well. It was recommended that sonic-log waveform data be acquired to confirm the magnetic measurements since it was expected that the magnetic data, while good for determining the nearest location along the

borehole and direction to the target, might have relatively poor distance discrimination. This is because during inversion or modeling of the magnetic data, the target casing has an unknown initial magnetization, making it difficult to calibrate the results.

Following acquisition and analysis of the MWD magnetic data, sonic waveform data were acquired. A single tool was used, consisting of three monopole sources with 13 receivers ranging from 11 to 17 ft and 0.5 to 6.5 ft offset, depending on which source was used during recording. Waveform traces were about 20 ms long sampled at 40 μs, totalling 512 samples each. Every receiver location comprised eight piezoelectric transducers arranged radially at 45° spacing around the tool body, making 13 × 8 = 104 traces available for each source activation with excellent azimuthal sampling. Figure 2 shows a diffraction observed on the waveform data coincident with the location of the magnetic MWD anomaly. The next steps were to confirm the direction and determine the distance to the target borehole.

Following acquisition of the sonic-log waveform data, elastic spectral element modeling was performed to confirm the response (Komatitsch and Tromp, 1999; Charara et al., 2013). Figure 3 shows a wavefield snapshot at 1000 μs with all wave modes including Stoneley, S-waves, and P-waves. The formation in the vicinity of the target borehole consists of anhydrite, which was assumed to be homogeneous (V_P = 6100 m/s and V_S = 3330 m/s) using properties derived from the sonic-log data. Two fluid-filled boreholes were embedded in the model at right angles to each other and separated by 2.4 m as indicated by preliminary traveltime analysis of the diffraction arrival on the sonic-log data. The source was a 9 kHz Ricker wavelet and data were modeled at a 40 μs sampling rate. A shot gather simulated at a position nearest the target borehole (Figure 4) shows diffractions the amplitude of which varies with receiver azimuth, confirming the sensitivity of the amplitude response to direction at sonic-logging frequencies using a real scale model of the tool sources and azimuthal receivers. Taking the difference between shots acquired with and without the target borehole (Figure 4) reveals arrivals scattered from the target borehole with relatively high amplitudes compared to P- and S-wave arrivals.

Similar modeling was performed for the case where the observation and target borehole are parallel (Charara et al., 2013). Successful matching of the modeled target reflection response with actual field data, including the azimuthal amplitude variations, provided confidence in processing and interpreting recorded data from the sonic logs.

Figure 5 shows the sonic waveform data for the orthogonal well case. Upgoing and downgoing reflections are visible on both raw shot gathers and common-offset sections. In this case, the relative amplitude ratios between Stoneley waves, S-waves, and P-wave reflections are about 100:10:1, respectively, for raw data. After band-pass filtering from 5000 to 15,000 Hz and frequency wavenumber (*f-k*) filtering in the common-offset domain to remove S-wave and Stoneley events, the relative ratios of the Stoneley, S-wave refractions, and P-wave reflections are approximately 10:2:1, respectively. Fortunately, the linear noise events are limited to a relatively narrow time interval from 2000 to 3000 μs. An unusual arrival that superficially resembles a diffraction is present (Figure 5: bottom) that has an apparent velocity at times similar to the formation velocity (20,000 ft/s). This "diffraction" is centered on the actual diffraction visible in Figure 2 and so provides a very visible indicator of the location of the nearby target. Once the target diffraction had been identified at the correct location along the borehole, the task became to determine which azimuth or direction the signal was coming from.

A common-offset section at the furthest source-receiver offset of 17 ft shows diffraction with a minimum two-way time of 1254 μs (Figures 2 and 6) coincident along the borehole with the magnetic anomaly detected during MWD logging. P-wave velocity was estimated from the sonic log at around 6100 m/s in this formation, indicating a minimum distance of 2.5 m to the location of the diffractor or target well. The strongest

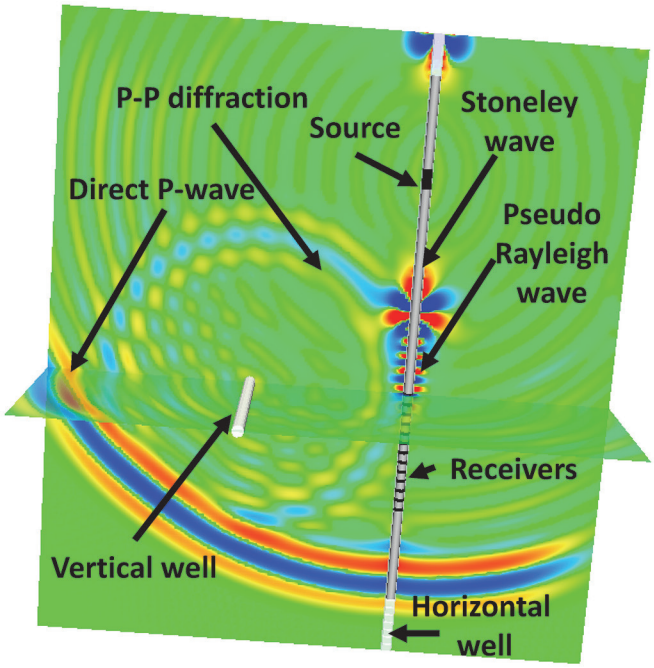

Figure 3. Elastic spectral element modeling of the sonic tool in a borehole showing the response of an adjacent orthogonal borehole and associated phases.

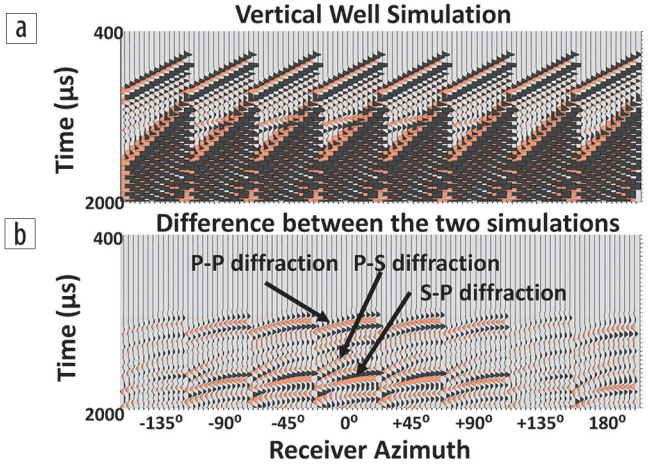

Figure 4. Elastic waveform modeling of a common shot gather with eight azimuthal receivers showing (a) the case with the adjacent borehole and (b) the difference between responses for the cases with and without the target borehole.

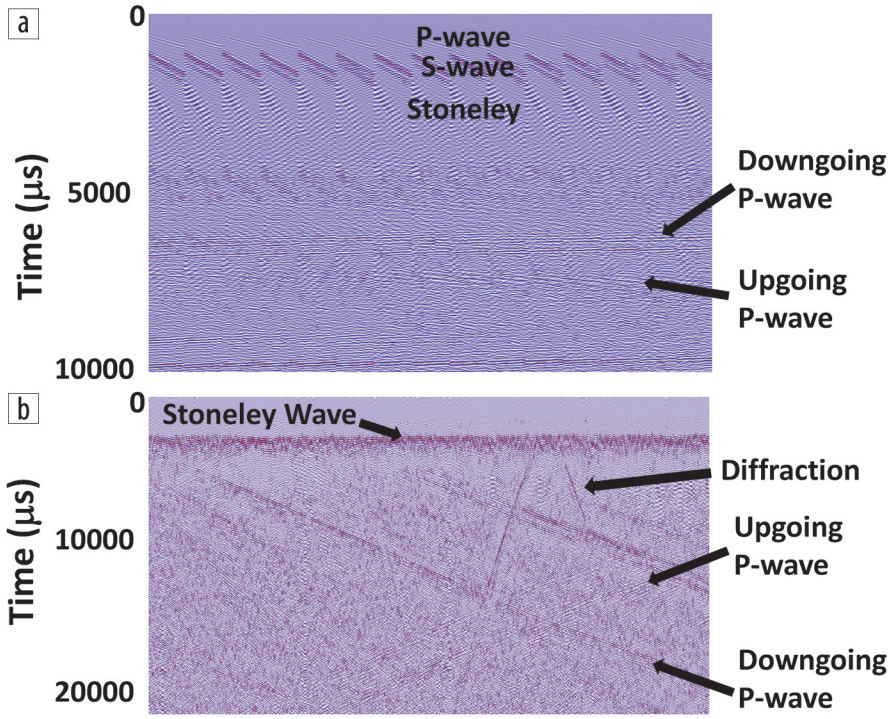

Figure 5. Sonic waveform data from the observation well including (a) raw common shot gathers and (b) a common-offset section after band-pass and *f-k* filtering to attenuate S-wave and Stoneley arrivals after summation of all radial components. Horizontal axis is positioned along the observation well for the common-offset section.

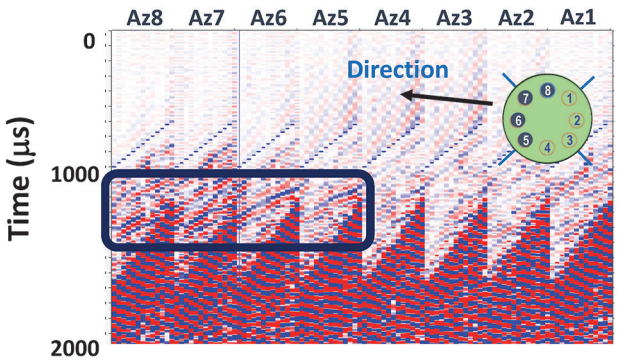

Figure 6. Common shot gather from the observation well sorted into eight azimuthal bins. The green circle is a cross section through the tool with the actual positioning of the azimuthal receivers at the location of the diffraction in the well. Receivers highlighted in blue indicate the side showing the strongest diffraction arrivals, which are also outlined by the dark blue box on the waveform data.

diffraction arrivals occurred on receivers on the west-facing azimuths, consistent with the passive magnetic sensing results. Since the acoustic ranging method was untried in this application, an initial sidetrack was drilled using the magnetic data as a guide (Figures 2 and 7). Additional MWD magnetic data were recorded during drilling of the sidetrack and revealed that the anomaly was closer (larger magnetic anomaly) but still in the same direction. On the second sidetrack, the target was overshot slightly (green curve in Figure 7) causing a large magnetic anomaly of opposite sign. A final sidetrack intercepted the target well at 2.4 m from the original observation well, at the location indicated by the initial acoustic data.

In addition to prestack data analysis, sonic waveform data can be used for imaging. The prestack waveform data can be processed much like a conventional 2D seismic line, the main difference being the need to perform prior wavefield separation. Conventional normal moveout-based velocity analysis is not required since velocity information is available directly from the sonic arrival times. After wavefield separation, upgoing and downgoing arrivals can be independently imaged in depth using prestack depth migration. In this case, a 2D phase shift plus an interpolation scheme was used. Downgoing arrivals are used to image events from reflectors above the borehole axis, while upgoing arrivals are used to image below the borehole. Due to the 3D nature of wave propagation, diffractions from objects out of the vertical plane along the axis of the borehole are also recorded. In this case, the formation boundaries are subhorizontal and parallel to the observation well, making imaging and interpretation very simple. We can conclude that reflection events in the depth-migrated sections (Figure 8) come directly from above and below the observation well. We can see clear reflections, which correlate well with bed boundaries recorded in well logs from the nearby target well at a resolution of better than 1 ft. In this case, due to low attenuation, the imaging depth is only limited by the recording time of the data, which in this case was 20 ms. The upper portion of the image is largely anhydrite with thin shale and dolomite stringers down to less than 1 ft thick, and the lowermost third in the deeper part of the section is dominated by interlayered limestones and dolomites. Gamma ray, electric, and neutron porosity logs from the target well are shown to scale for comparison purposes. The high velocity and hence low attenuation of these formations has clearly aided in acquiring high signal-to-noise ratio reflection data at relatively large two-way times.

Case study 2: Locating a vertical well from a nearby vertical well

In a second test, the objective was to detect a vertical cased borehole that was cement filled for abandonment purposes from a nearby subvertical well (Figure 9). Even though the formations here are horizontal as in the first test case, they exhibit large vertical velocity variations over the interval of interest (Figure 9a). Since the target borehole was cement filled, this reduced the impedance contrast between the formation and the wellbore, in contrast to the previous example where the target well was fluid filled. Well survey and magnetic ranging data indicated that the target borehole was about 6–7.6 m from the observation well (Figures 9c and 9d). Due to the larger distance to the target in

this example, it was expected that reflected/scattered energy from the well would be much weaker and arrive in the same time window in which strong refracted S-waves are recorded on the sonic waveform data. The generally lower formation velocities and consequently higher attenuation in these formations will also further reduce the reflection signal strength. As an added complication, reflections from the target in this configuration are expected to have similar moveout as a function of source-receiver offset as the refracted P-waves, S-waves, and Stoneley arrivals in the common-offset/receiver gathers. This configuration makes noise removal without damaging reflected events more challenging. Unlike the previous example, it was not possible to unambiguously identify the reflected energy on prestack data.

Nevertheless, after noise removal on the common shot gathers and migration, an image was obtained that is generally consistent with the expected location of the target borehole (Figure 9b). The high-amplitude red event in the lower section is interpreted as an image of the target well, even though it seems close to the band of migrated residual S-waves seen as the blue area in the section above. If the red event would be simply migrated residual shear waves, then there would no reason for it to decay in amplitude in the section above. The migrated image shows that the high-energy event is only present in the lower section where a relatively fast limestone was encountered. This suggests that the acoustic impedance contrast between the cement-filled borehole and formation is sufficiently high in the fast formation, but too low in the slow formations above to generate a visible reflection/diffraction. Since the strength of the scattered signal is proportional to the impedance contrast, and the migration image strength is consistent with the P-wave velocities from log data, this suggests that the observed event is real and not an artifact.

Based on the borehole velocity profile and picked arrival times of the reflected event, the distance to the target well is estimated to be between 6 and 6.5 m from the survey well (Figure 8b). These distances are in close agreement with those estimated from gyro surveys of both wells (Figure 8d) as well as the results from active EM ranging conducted in this borehole (Figure 8c), further supporting the conclusion that the amplitude change in the image results from diffracted energy from the nearby cement-filled cased borehole.

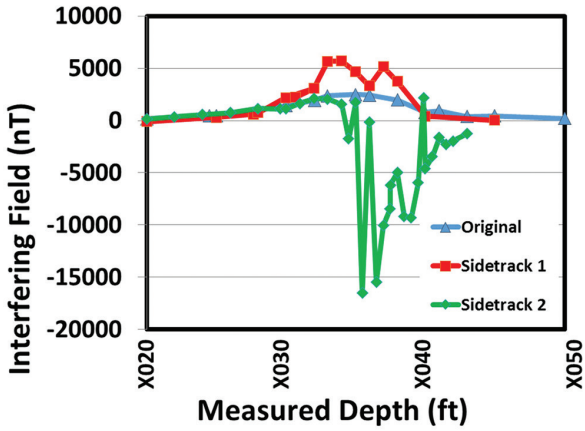

Figure 7. Passive MWD magnetic data showing three runs in different laterals. The approximate location of the nearby vertical casing is at a measured depth of X036 ft. Note the initial positive anomaly, which became a large negative anomaly on sidetrack 2 as the well slightly overshot the target casing.

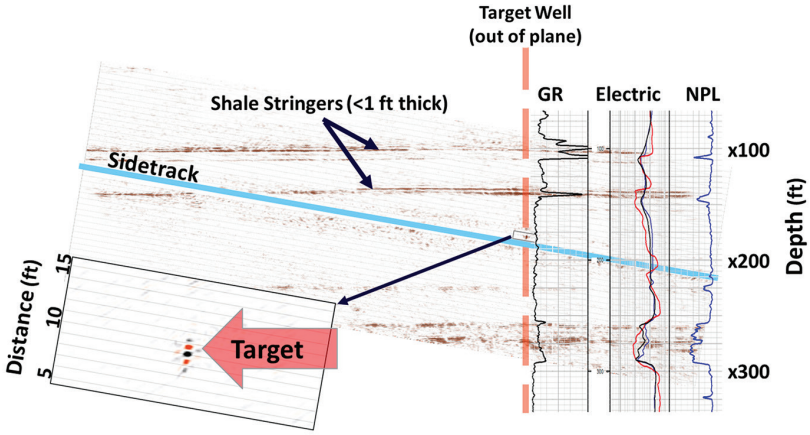

Figure 8. Prestack depth migration imaging using acoustic data after band-pass and *f-k* filtering to remove noise. Reflectors are visible up to 100 ft (30 m) above and below the observation well. An expanded view shows a nearby vertical cased borehole at about 9 ft (2.7 m) from the observation well imaged as a point diffractor.

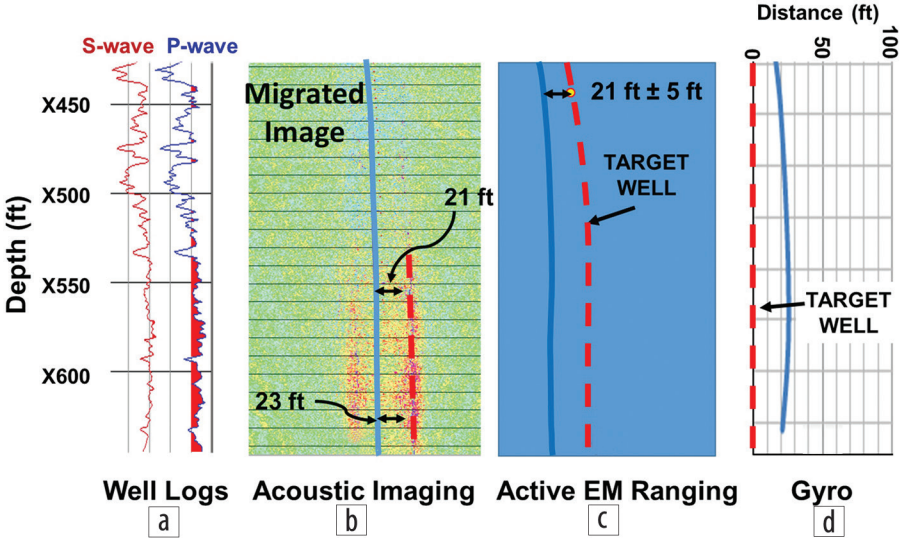

Figure 9. The second case study showing (a) sonic logs, (b) the migrated reflection data from the full-wave sonic logs, (c) results from active ranging, and (d) drilling data from gyroscopic surveys. The high-amplitude (red) migrated event in (b) is interpreted to be an image of the target borehole.

Table 1. Summary of the performance of different well-to-well ranging methods for two different scenarios.

	Orthogonal wells	Parallel wells
Mud type	Water based	Oil based
Target well cemented	No	Yes
Host rock	Very fast (anhydrite)	Variable velocity (shales, sandstone, limestone)
Acoustic imaging distance	2.4 ± 0.25 m	6.25 ± 0.6 m
EM ranging distance	1.6 ± 0.4 m	6 ± 1.6 m
Acoustic detection	Pre- and poststack	Poststack
Deep reflection imaging	> 100 ft depth	None — bedding perpendicular to acquisition

Summary

A new application of single-well acoustic imaging was presented for detecting the distance and direction to a target borehole. This result was consistent with MWD passive magnetic data in terms of location and direction to the target borehole, but was more accurate in terms of predicted distance to the target for the case where the boreholes were orthogonal (Table 1). These results were later validated by drilling. For the case where the boreholes are subparallel, acoustic data can be noisy and may require imaging before interpretation. While acoustic single-well imaging can detect boreholes without magnetic or conductive casing and can work in configurations where active EM ranging is poor, magnetic and EM methods can perform well in cases where the boreholes are subparallel at generally greater distances than acoustic methods. EM and magnetic methods are not adversely affected by the presence of cement in the borehole, which may reduce impedance contrast with the surrounding formation, though it would limit access to the target for active EM ranging. A disadvantage of single-well acoustic imaging is that it requires a separate logging run unlike MWD magnetic data acquisition, which can be acquired without suspending drilling operations. It is clear that acoustic and EM methods are complementary and can be jointly utilized for determining direction and distance to a target borehole. TLE

Acknowledgments

We would like to thank Saudi Aramco for permission to publish this work.

Corresponding author: michael.jervis@aramco.com

References

Charara, M., M. Jervis, D. Sabitov, and I. Selznev, 2013, 3D spectral element modeling for acoustically sensing a well from a nearby well: 75th Conference and Exhibition, EAGE, Extended Abstracts, https://doi.org/10.3997/2214-4609.20130228.

Esmersoy, C., C. Chang, M. Kane, R. Coates, B. Tichelaar, and E. Quint, 1998, Acoustic imaging of reservoir structures from a horizontal well: The Leading Edge, **17**, no. 7, 940–946, https://doi.org/10.1190/1.1438075.

Haldorsen, J. B. U., A. Voskamp, R. Thorsen, B. Vissapragada, S. Williams, and M. Fejerkov, 2006, Borehole acoustic reflection survey for high resolution imaging: 76th Annual International Meeting, SEG, Expanded Abstracts, 314–318, https://doi.org/10.1190/1.2370182.

Hornby, B. E., 1989, Imaging of near-borehole structure using full-waveform sonic data: Geophysics, **54**, no. 6, 747–757, https://doi.org/10.1190/1.1442702.

Jervis, M., A. Bakulin, T. Tonellot, I. Ghamdi, A. Shabbir, and H. Yamamoto, 2012, High-resolution seismic imaging from a single borehole to detect a nearby well: 82nd Annual International Meeting, SEG, Expanded Abstracts, 1–4, https://doi.org/10.1190/segam2012-0963.1.

Komatitsch, D., and J. Tromp, 1999, Introduction to the spectral element method for three-dimensional seismic wave propagation: Geophysical Journal International, **139**, no. 3, 806–822, https://doi.org/10.1046/j.1365-246x.1999.00967.x.